

Turbulence, waves and mixing at shear-free density interfaces. Part 2. Laboratory experiments

By J. L. McGRATH¹†, H. J. S. FERNANDO¹‡
AND J. C. R. HUNT²§

¹Environmental Fluid Dynamics Program, Department of Mechanical and Aerospace Engineering,
Arizona State University Tempe, AZ 85287-6106, USA

²Meteorological Office, London Road, Bracknell, Berkshire RE12 2SZ, UK

(Received 2 February 1996 and in revised form 19 May 1997)

A laboratory experimental study was performed to investigate turbulence, waves and mixing at a sharp density interface (with a jump in buoyancy Δb), subjected to shear-free turbulence induced by oscillating grids with typical velocity and length scales of u_H and L_H , respectively. The cases where turbulence is present on one side (single-sided stirring) or on both sides (double-sided stirring) of the interface were considered. Extensive flow visualization studies and quantitative measurements were performed on the motion field and mixing characteristics at the interface. It was found that, rather than any one mechanism controlling the mixing process, different mechanisms (namely engulfment, generation of waves and their breaking, eddy impingement and Kelvin–Helmholtz billows) play dominant roles over different ranges of the bulk Richardson number Ri ($Ri = \Delta b L_H / u_H^2$). For the Ri range where wave generation is significant, certain hypotheses and predictions of the companion paper by Fernando & Hunt (1997) were tested in detail, by flow visualization studies of the qualitative properties of interfacial motions and quantitative measurements of the r.m.s. fluctuations of interfacial velocity and displacement, the local gradient Richardson number within the stratified layer, the frequency spectra and the related fractal properties of the interface. The results are consistent with the hypothesis that, at high values of Ri (> 35), the density interface consists of linear internal waves driven by turbulence at high frequencies and breaking waves with sharp horizontal gradients of density at low frequencies.

1. Introduction

Engulfment, eddy impingement, Kelvin–Helmholtz (K-H) billowing and breaking of internal waves are some of the different mechanisms that have been proposed to explain the interaction between the motions within thin stably stratified horizontal inversion layers and within adjoining regions of turbulence which may be on one or both sides of the stratified layer. The nature of these interfaces depends on the dynamical

† Present address: Department of Mechanical Engineering, Massachusetts Institute of Technology, Cambridge, MA 02139, USA.

‡ Author to whom correspondence should be addressed (e-mail: J.Fernando@asu.edu).

§ Present address: Department of Applied Mathematics and Theoretical Physics, University of Cambridge, Silver Street, Cambridge CB3 9EW, UK.

state of the flow or on the bulk Richardson number Ri , which is characterized by the ratio of the restoring buoyancy forces associated with the deflection of the inversion layer and the vertical inertial forces of turbulence (Fernando 1991). The bulk Richardson number is defined as $Ri = \Delta b L_H / u_H^2$, where Δb is the characteristic buoyancy jump across the stratified layer and u_H and L_H , respectively, are the r.m.s. velocity and the integral lengthscale of turbulence. Only a few of these proposed mechanisms can occur at the same value of Ri simultaneously in the same flow, and therefore they are best related to each other when considered in groups corresponding to different ranges of Ri .

This is the approach used to analyse the experiments described in this paper. The experiments are put into context by comparing them with different types of motion fields that occur at shear-free density interfaces. Such motion fields were discussed in the companion paper by Fernando & Hunt (1997, hereafter referred to as F & H), and include: (i) passive movement of the interface in the single-sided stirring case at low Ri , dominated by engulfing motions and determined by the transition of the fluctuating motion from turbulence to irrotational motions above the inversion layer (Phillips 1955; Townsend 1976); (ii) as Ri increases, the generation of either small-scale 'wispy' motions as a result of eddy impingement on the interface that determine the mixing (Linden 1973) or eddies 'scraping' along the interface which induce a local Kelvin–Helmholtz instability (Mory 1991); and, (iii) with further increases in Ri , the generation of waves travelling on and within the interface that grow until they break and cause small-scale turbulence and mixing (Hannoun & List 1988; Drazin 1969).

The internal-wave-dominated regime (iii) is of special interest for this paper and this regime is shown to occur when $Ri > 35$. The wave growth is partially resisted by the gradients of fluctuating Reynolds stresses which are caused by the large-scale straining of the induced wave motions acting on small-scale turbulence (Phillips 1959; Carruthers & Hunt 1997). The breakdown of the waves may occur: (a) due to the fluctuations in the density gradient because they may be large enough to reverse the stable density gradient and force it to be locally unstable (i.e. $Ri_g < 0$, where Ri_g is the local gradient Richardson number), leading to a rapid breakdown or overturning of waves by static instability (Orlanski & Bryan 1969; Carruthers & Hunt 1997) or (b) due to large fluctuations in the local velocity gradient, which may lead to a shear or local Kelvin–Helmholtz instability when $0 < Ri_g < 1/4$ is satisfied. (Note that these K-H instabilities are different from those due to scraping motions discussed in (ii).)

When examining data of breaking waves, it is instructive to recall that the clearest example of such motion is probably the head of an intrusion propagating along a density interface (Simpson & Britter 1979). We find that on long lengthscales interfacial motions driven by turbulence have some similarities to a set of interacting intrusions! The geometric form of the interface caused by wave breaking, particularly its maximum slope, lengthscales and timescales between breaking events, are critical elements in the construction of the model of F & H. Note also that, in a breaking wave, very small-scale turbulence is generated which is therefore not closely correlated to that in the turbulent region which has already generated the waves.

In experimental studies of these and other inhomogeneous turbulent stratified flows, flow visualization techniques are an essential means of elucidating the imprints of the eddies and waves and distinguishing between different entrainment mechanisms which correspond to distinct patterns of motion on the interface. Although a number of laser-induced fluorescence (LIF)-based visualization studies of turbulent interfaces have been performed previously, only Perera, Fernando & Boyer (1994) have used this technique to delineate the different regimes (i), (ii) and (iii). In this paper we extend their study, which focused on thick inversion layers, by analysing time sequences of

motions on their interfaces, a technique used for turbulent flows by Hussain & Clarke (1981).

Two other techniques were also used in the study of the instantaneous structure of the interface. By measuring the local density and velocity gradients, then calculating the local value of Ri_g , the presence of conditions suitable for rapid growth of waves and their breaking by static instabilities is determined (when $Ri_g < 1/4$ and $Ri_g < 0$, respectively). Also, the nature of the waves, when they break, can be inferred from the time traces of $Ri_g(t)$, from our other technique of fractal analysis of the interfacial density contours of the interface and from the results of statistical spectral analysis of the same quantity.

To examine in more detail the qualitative aspects of the proposed mechanisms and to test the models, it is also necessary to make detailed statistical measurements. The model of F & H depends sensitively on the assumption that motions at the interface have qualitatively different forms in the high-frequency (ω) range (when they are linear waves responding to the turbulent forcing) and in the low-frequency range (when they have a nonlinear structure determined by the growth and breaking of waves). The critical deductions from the model are the velocity and displacement variances at the interface as a function of Ri and the form of the displacement spectra $\psi_d(\omega)$ in the low-frequency nonlinear range, which are determined by the assumption that wave breaking involves inversion-layer overturning (whence $\psi_d(\omega) \sim \omega^{-2}$). This contrasts with the prediction $\psi_d(\omega) \sim \omega^{-3}$ of Phillips (1977) for breaking lowest-internal-wave modes on a thin interface in the absence of turbulent forcing; the latter has been used by Hannoun & List (1988) as a reference theory for analysing the wave-amplitude spectral results of their experiments on turbulent mixing in thin inversion layers.

In this paper, the results of a series of laboratory experiments performed on turbulent motions at shear-free thin density interfaces are described. The experiments of Hannoun & List (1988) in which only one side of the interface was turbulent (single-sided stirring) are repeated to establish the validity of the present results and to extend their measurements. Then experiments with turbulence on both sides of the interface (double-sided stirring) are reported; there are only limited velocity data on this case, by McDougall (1979). In McDougall's experiment the fluid was withdrawn and added to the turbulent layers to maintain a steady state, which implicitly introduces a stabilizing buoyancy flux to the fluid system; in this case, as was discussed by Fernando & Long (1988), the interfacial properties are fundamentally different from the no buoyancy-flux case.

This paper is arranged as follows. In §2, the experimental procedure is discussed. This is followed by qualitative observations (§3) and quantitative measurements (§4). The conclusions of the study are given in §5.

2. Experimental method

The test apparatus is a conventional mixing box, similar in construction to that employed by Turner (1968), among others; see figure 1(a) for a schematic diagram. The tank dimensions were 25 cm \times 25 cm \times 60 cm. Two monoplanar horizontal grids which could be vertically oscillated were located 7 cm below the water (free) surface and 12 cm above the bottom of the tank and the distance between the grids was 38 cm. The grids were made of 1 cm square Plexiglas rods, glued to form a square mesh of size $M = 5$ cm. The solidity of the grid was 38%.

The grids could be independently oscillated using separate slider-crank mechanisms. For the present experiments, however, both grids were oscillated out of phase with

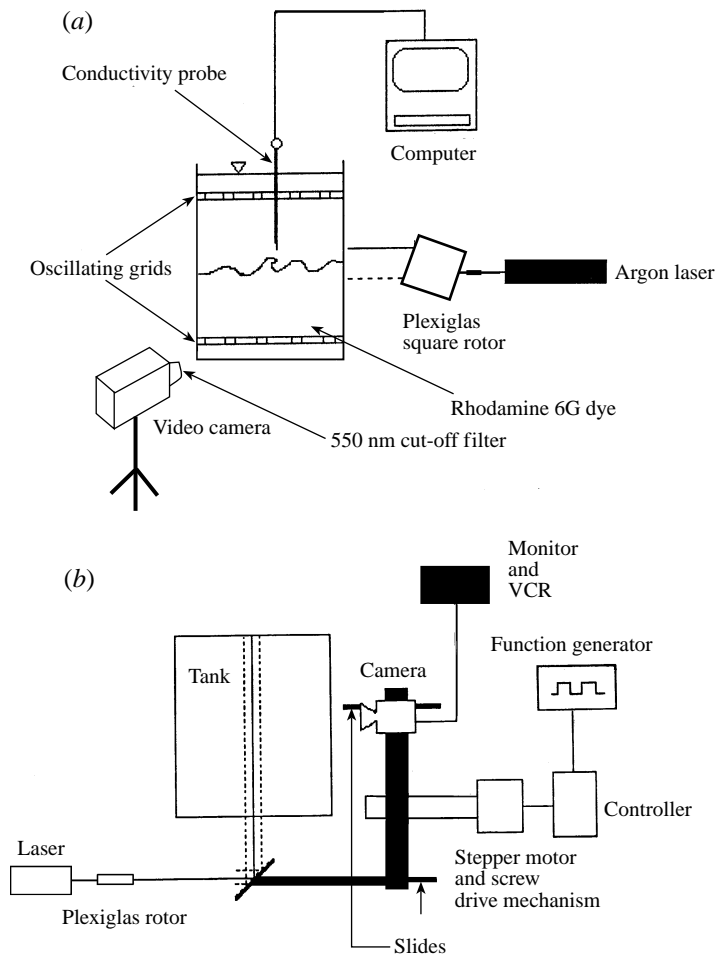


FIGURE 1. Schematic diagrams of the experimental set-ups. (a) The set-up used to capture the three-dimensional spatial-temporal behaviour of the interface. (b) Top view of the apparatus used to examine the three-dimensional spatial structure of the interface.

similar strokes and frequencies; thus the forcing of turbulence was approximately symmetrical with respect to the mid-plane between the grids. A stroke of 2.15 cm was used in all experiments. The desired Richardson numbers were obtained by varying the density jump ($\Delta\rho$) across the interface and the grid-oscillating frequencies (f) in the ranges $3 \times 10^{-3} < \Delta\rho < 8 \times 10^{-3}$ (g cm^{-3}) and $2 < f < 3.8$ (Hz), respectively.

As a reference for the later stratified experiments, a series of experiments was carried out in fresh water. Either one or the other grid was oscillated with prescribed strokes and frequencies, and the resulting turbulence field was measured using a single-component laser-Doppler velocimeter (LDV). Both the horizontal (u_H) and vertical (w_H) r.m.s. turbulent velocities were measured separately at different distances away from the grids. These measurements were in general agreement with the experiments of Hopfinger & Toly (1976) and DeSilva & Fernando (1992). In addition, the velocity-time traces were used to calculate the Eulerian integral timescales τ_H , from which an integral lengthscale L_H could be estimated as $\tau_H u_H$ (typically, near the interface, $\tau_H \sim 4$ s, $L_H \sim 2$ cm and $u_H \sim 0.5 \text{ cm}^{-1}\text{s}$).

During the setting up of stratification experiments, the tank was filled with two layers using a Rhodamine 6G-mixed salt solution in the bottom layer and an aqueous alcohol solution in the top layer. The salty layer was first put into the tank and then the aqueous alcohol solution was carefully released onto a sponge that was floated on the salty layer. The upper fluid slowly spread on the bottom layer causing minimal mixing. Since the molecular diffusivities of salt and Rhodamine G are approximately the same, the changes of the salt concentration could be monitored by tracking the concentration of Rhodamine. The density interface was initially located at the mid-depth between the grids. Concentrations of salt and alcohol were selected so as to yield a uniform refractive index over the entire depth of the fluid column; see Hannoun, Fernando & List (1988) for details. Measurements were taken 5–10 min after the grids were set in to motion. This allowed sufficient development time for the nonlinear dissipative interfacial waves to grow and break, which has a local timescale of a few seconds, and for the whole turbulence field to adjust (see Kit, Strang & Fernando 1997).

Quantitative flow visualization of the stratified experiments was performed using the laser-induced fluorescence (LIF) technique. As is shown in figure 1(a), a uniform-intensity 6 cm tall vertical sheet of Argon-ion laser light was generated by passing a laser beam through a rotating square prism. Considering the required resolution, turbulence scales near the interface and possible wall influence, it was decided to use a horizontal imaging field of 8 cm, located symmetrically with respect to the centre of the tank. The data so obtained in a central plane are expected to be representative of the entire interface, except near the sidewalls of the tank where wall effects may play a significant role. Further details on this laser-scanning technique are given in DeSilva, Montenegro & Fernando (1990). (Replacement of tank wall sections with high-quality optical glass yielded a good-quality uniform laser sheet without the effects of Plexiglas imperfections.) The Rhodamine dye fluoresces at 570 nm when exposed to 514 nm emission of the Argon-ion laser. The fluorescent light was collected at a normal direction to the light sheet, on a 1.25 cm, 512×488 , CCD array, after passing through a 550 ± 10 nm high-pass cut-off filter to remove 514 nm light. The resulting image featured a sharp contrast in the light intensity of the fluid layers. The images from the video records were digitized at 8-bit grey-scale resolution and 512×479 pixel resolution using an Imaging Technology Inc., PC-Vision Plus, Frame Grabber board.

The dye concentrations used did not exceed 140 p.p.b. At this concentration, the intensity of the fluorescent light is proportional to the concentration of the dye; the attenuation of the beam intensity over the 8 cm horizontal dimension of the field of view was less than 8%, and could be easily accounted for in the data analysis. Extensive discussions on the use of fluorescent dyes for monitoring concentration, the response of dyes to light intensity at different concentrations and corrections for beam attenuation are given in Liu *et al.* (1977), Koochesfahani (1984), Koochesfahani & Dimotakis (1986), Hannoun & List (1988), Papantoniou & List (1989) and Stephenson & Fernando (1991).

Constant-light-intensity contours measured at a given time t could therefore be considered as constant-density contours. In a method similar to that employed by Hannoun & List (1988), light intensities (I), expressed by the non-dimensional variable $\alpha(x, t)$, were used to identify these contours,

$$\alpha = \frac{I - I_l}{I_u - I_l},$$

where I_u and I_l are the average light intensities in the upper and lower layers,

respectively. Constant- α contours were constructed by scanning a pixel column from low α to high α , recording the first pixel coordinate at which α exceeded or met a specified threshold, and appending the results of adjacent column scans.

The r.m.s. displacement of a given α -contour in the interfacial region was determined by measuring the interfacial displacement at each pixel column relative to the mean interface position. The r.m.s. interfacial velocities were computed by measuring the movement of a contour over a 334 ms time interval (11 frames). This time difference was selected so as to avoid a highly discretized velocity record resulting from smaller time differences, while maintaining a sufficiently small time step in comparison to the eddy-turnover timescale τ_H . The sensitivity of the velocity measurements to the number of frames (n) used was found to be insignificant for $4 > n > 15$. When $n < 4$, the movements of α -contours were often not sufficiently large to yield displacements appreciably larger than the instrument noise; and when $n > 15$, the time interval appeared to be too large to define an instantaneous velocity (i.e. the calculated velocity depended on n).

The contours were passed through a fifth-order digital Butterworth (low-pass) filter with a cut-off wavenumber of 63 cm^{-1} , so as to eliminate high frequency noise without affecting the relevant turbulence statistics. Since the vertical scan of a pixel column terminates at the first desired α -value, inversions created by overturning waves and ensuing turbulent patches caused gaps in the contours that would lead to fallaciously high velocities if their effects were not rectified. The digital filter lessened the effects of small inversions by connecting contour fragments. It was still necessary to avoid frames with substantial wave breaking events and separated turbulent patches for the calculation of turbulence statistics. The instantaneous interfacial-layer thickness h was defined as the averaged vertical distance between the $\alpha = 0.2$ and $\alpha = 0.8$ contour lines. For a given Richardson number, the data from at least 20 frames were used in calculating the statistics, which amounted to more than 6000 data points; horizontal homogeneity of the flow was assumed in the calculations. The statistics were found to converge, with a standard deviation of the means of less than 7%.

The local gradient Richardson number in the interfacial zone, defined as $Ri_g = (\Delta b / \Delta z) / (\Delta u / \Delta z)^2$, where u and b are instantaneous horizontal velocity and buoyancy measurements and z is the vertical coordinate, was measured with a vertical resolution of $\Delta z = 2.7 \text{ mm}$ using a novel instrument named the 'local Richardson-number probe'; further details of this instrument are given in DeSilva (1991). In this instrument an in-house-built dual-probe-volume laser-Doppler velocimeter (He-Ne) is used for horizontal velocity measurements and a custom-manufactured (by Precision Measurements Inc.) dual-tip four-electrode conductivity probe is used to measure the buoyancy difference; both the LDV and conductivity probe volumes have a vertical separation of 2.7 mm.

The three-dimensional nature of the interface was studied in several experiments. In these, the laser sheet traversed the tank, as in laser tomography, to give a three-dimensional picture. The apparatus used for this study is schematized in figure 1(b). The laser sheet generated by the scanner was directed into the tank by a high-quality front surface mirror placed at 45° to the incoming beam. The mirror and a video camera were mounted atop a lightweight aluminium structure, which was fitted with precision roller bearings and constrained to move along precision guide rails. A computer-controlled stepper motor and lead-screw arrangement traversed the platform, causing the laser sheet to sweep through a volume inside the tank while maintaining a constant distance between the camera and laser sheet so that the field of view is maintained constant. The motor controller was driven by a square-wave

function generator. The frequency of the square wave and the resolution of the lead-screw (144 steps/inch) determined the velocity of the sweep. The video signal from the camera was sent to a VHS recorder and a monitor. To optimize the image resolution, a sweep velocity of $11.4 \text{ cm}^{-1} \text{ s}$, determined by the e^{-2} beam thickness at the centre of the tank (0.06 cm) and the 60 Hz field rate of the camera, was used. This velocity is much greater than the r.m.s. velocities of the mixed-layer eddies (typically of the order of $0.5 \text{ cm}^{-1} \text{ s}$). In addition, the scan duration was limited to times well below the eddy-turnover time, $\tau_H \sim 4 \text{ s}$, and the convective contributions to the three-dimensional data were estimated to be less than 15%. The errors in the experimental data were calculated using the standard technique of Moffatt (1988), and the error bars are included in the graphs. Further details of this set-up are given in the report by McGrath, Fernando & Montenegro (1993).

3. Qualitative observations

Extensive flow visualization studies were made to delineate the mixing mechanisms that are active in various Richardson number ranges. To this end, consecutive frames of video recordings were analysed using the LIF technique, and possible mixing mechanisms were identified. These observations are discussed below.

Although no experiments were performed with initial $Ri \leq 1$, the processes occurring at the interfaces were evident during the observations made in a few double-sided stirring experiments, wherein the density difference between the layers was allowed to decrease until the system runs down to a homogeneous fluid column. Just before homogenization, the interface breaks down into fragments, which are transported by the eddy motions into the turbulent layers. In the experiments carried out with higher Ri , as figure 2(a) shows for the single-sided stirring case with $Ri \approx 12$ (with turbulence in the upper layer), the movement of the large eddies normal to the interface is significantly reduced by buoyancy forces and these eddies rebound back into the turbulent layer, carrying, as they move, some fluid with them from the dense layer. As the dense fluid parcels are entrained, they are broken up by the turbulent eddies and mix within the layer. Linden (1973) first suggested eddy impingement as the key entrainment mechanism for shear-free density interfaces, but he did not indicate the range of Ri in which it predominates over other mechanisms. Our detailed observations suggest that this range lies between $1 \leq Ri \leq 15$. As this upper limit is approached, signs of shearing off of the interface by the eddies penetrating into the interface is evident, in addition to the presence of rebounding eddies. As discussed below, this shearing mechanism becomes dominant at $Ri > 15$. A possible shearing event is shown in figure 2(a) at $Ri \approx 12$, where on the right-hand-side eddies travelling to the left and right across the interface can be seen to be pinching off a segment of the interface. As shown in figure 2(b), at times the interface with double-sided stirring ($Ri \approx 12$) can be more fragmented than the single-sided stirring interface. Such events, however, are infrequent and typically the two flow situations showed somewhat similar appearances. In the double-sided stirring case, eddies from both sides can interact so as to break up the interface; this effect is pronounced when one energy-containing eddies from each side impinge approximately at the same location. (According to Turner 1968, such interactions are rare and both sides can be considered as statistically independent.) Our records indicate that the occasional marked fragmentation of the interfaces caused by double-sided stirring ceases when $Ri \geq 20$, and thereafter the eddy shearing effect was the major mixing mechanism. F & H predicted that the conditions for the occurrence of K-H instabilities by 'sloshing' of eddies over the

interface can be present when $Ri < 15$. Such instabilities, however, were rare due to the dominance of other more efficient mixing mechanisms (see figure 5c of F & H).

As stated above, under more stable conditions, typically when $Ri > 15$, the eddies with significant horizontal velocities penetrate into the interface, scour it and shear off heavy fluid parcels into the mixed layer. This variant is clearly demonstrated in figure 3(a) (single-sided stirring, $Ri = 35$). Here, two mixed-layer eddies (red fluid lumps) moving horizontally and perpendicularly into the illuminated plane have apparently penetrated and disrupted the interface. In so doing, the two eddies have merged and severed off the interfacial fluid. These severed fluid parcels are distorted by and molecularly mixed with mixed-layer turbulence, thus homogenizing with the background. Observations suggest that this mechanism dominates mixing at the interface in the range $15 < Ri < 35$, although such events are not absent beyond this range. A dominant eddy-shearing event at $Ri = 24$ for the double-sided stirring case is shown in figure 3(b). Also, it is evident that any travelling waves on the interface produced by these motions are weak compared to the interfacial distortions produced by impinging eddies.

When $Ri > 40$, entrainment in both single- and double-sided cases is completely dominated by interfacial waves and their breaking. These events are shown in figure 4(a) (i, ii), for single- and double-sided stirring for $Ri \approx 52$. These interfacial waves travel along the interface moving in random directions at velocities comparable to the r.m.s velocity u_H , and as they do so they are sufficiently intermittently amplified that the interface steepens and then breaks into fragments. Because of this particular type of movement and amplification (which we studied on a video) their breaking can be differentiated from the splashing and piercing mechanism described earlier. Some waves (in cases where the interface is thicker) are similar to intrusions and others take the form of a train of overturning structures. For the single-sided case, wavy disturbances and their breaking can be identified when $Ri > 30$, but these wave forms are often disturbed by eddies that pierce through the growing waves. This phenomenon is less evident for the double-sided case for $Ri < 40$. Note that the typical horizontal distance the waves travel before they break or decay is of the order of 2–5 cm, which is of the order of the integral lengthscale L_H .

An individual wave breaking event is demonstrated in the photographs shown in figure 4(b), for a single-sided stirring case at $Ri \approx 52$. The frames are taken about 1/3 s apart. It is clearly seen that the local interfacial-layer thickness (as measured from the transition between the heavy red fluid and lighter blue fluid) is spatially varying, and grows as a result of intermittent local events involving interfacial distortions and mixing. In figure 4(b) (i), the red patch next to the region marked by X appears to be a remnant of a previous breaking event, and a growing wave is indicated by Y. Note the four stages of the turbulent mixing event depicted in figure 4(b) (i–iv): (i) the growth of the wave or billow Y, probably caused by horizontal motions above the interface; (ii) the partial severing off (Y_1) from the interface; (iii) the density of the distorted tongues of the interface, via turbulent mixing, tends to achieve the density of the surrounding fluid (this can be seen by the change in the colour of the tongue from red to blue); and (iv) the falling back of a part of the originally entrained fluid on the interface, Y_2 . The slumping of partially mixed fluid elements back onto the interface appears to make a significant contribution to the evolution of the interfacial layer. Note that the change of density within the tongue-like element of the breaking event is quite rapid possibly because of the prevailing high strain rates. While the two fluids molecularly mix across the turbulent/non-turbulent boundary, the background and internal strains elongate the wave, continuously sharpen the scalar gradient

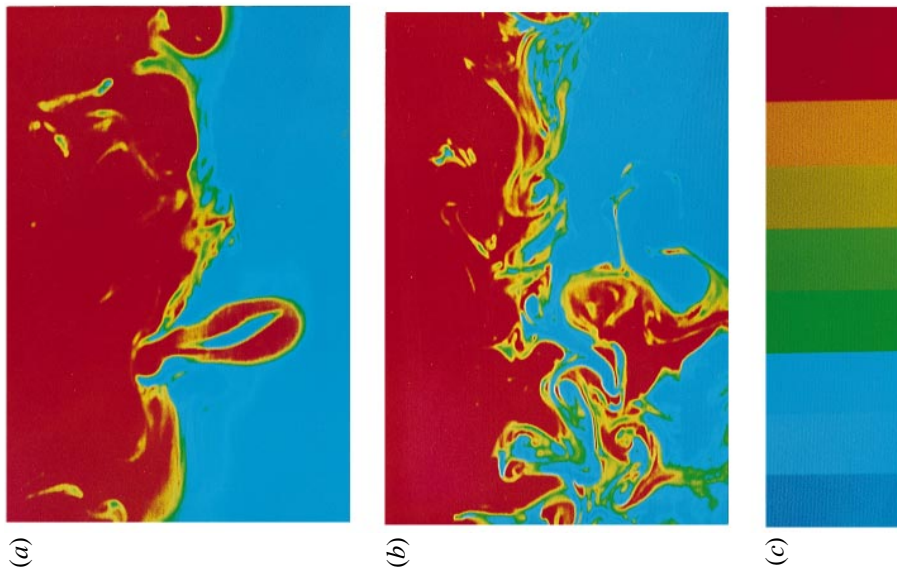


FIGURE 2. The nature of the interface at $Ri \approx 12$. (a) Single-sided stirring. (b) double-sided stirring. (c) Pseudocolour representation used to represent the concentration.

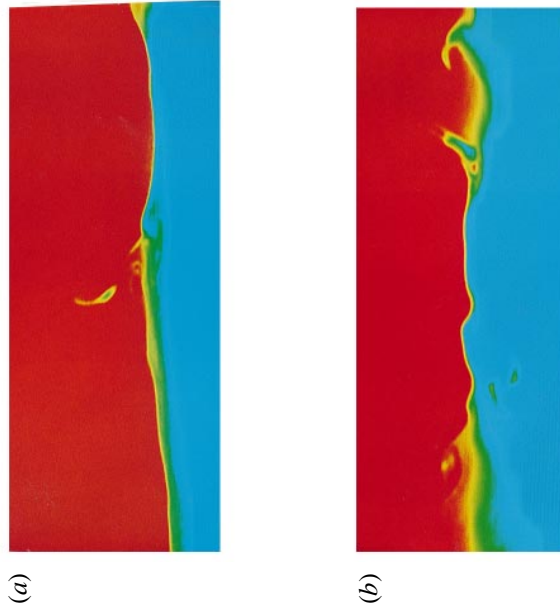


FIGURE 5. Wave breaking at high Ri . (a) Single-sided stirring, $Ri = 95$; (b) double-sided stirring, $Ri = 90$.

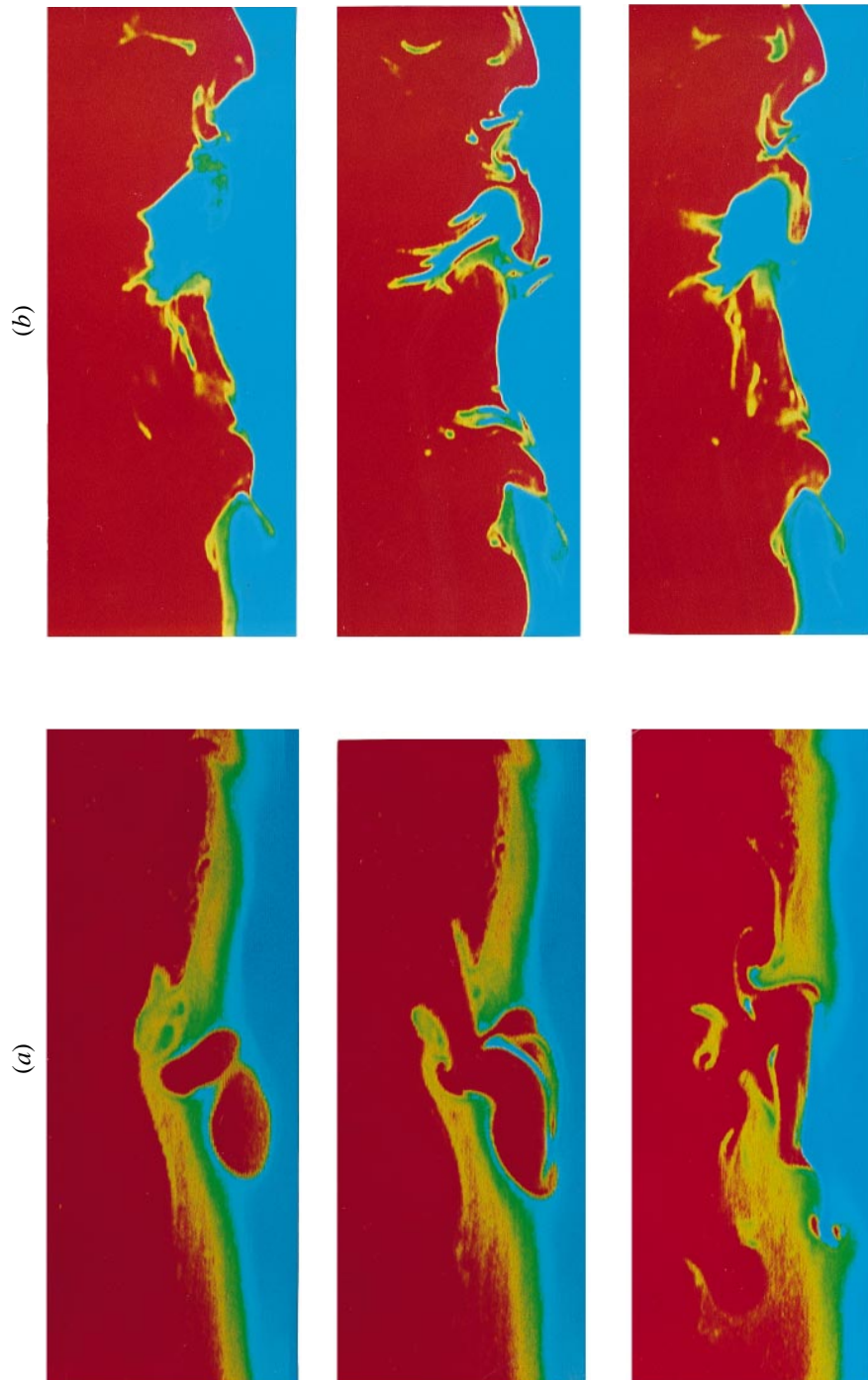


FIGURE 3. Entrainment by eddy shearing. (a) Single-sided stirring, $Ri = 35$. Photographs were taken consecutively with time differences of 165 ms. (b) Double-sided stirring, $Ri = 24$. Photographs were taken consecutively with time differences of 330 ms.

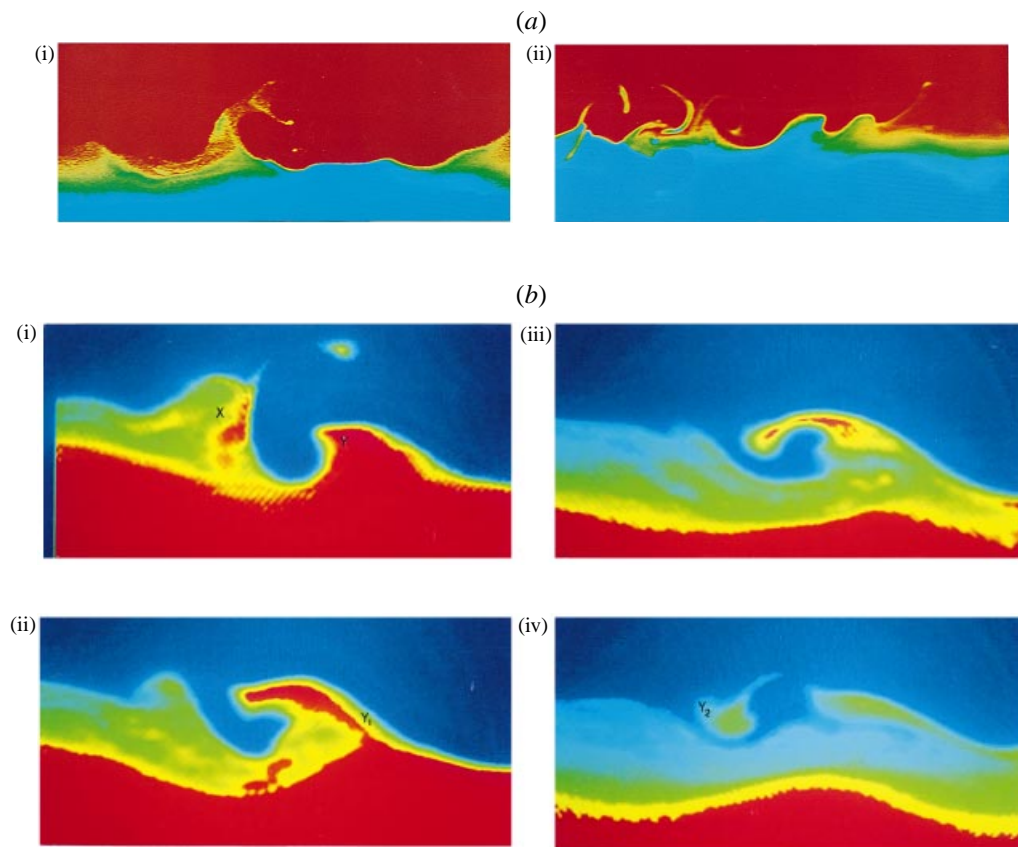


FIGURE 4. (a) Structure of the interface at $Ri \approx 52$. (i) Single-sided stirring, (ii) double-sided stirring. (b) (i-iv) Time-lapse photographs of an individual-wave breaking event in single-sided stirring at $Ri \approx 52$. Labelled points are explained in text.

region and increase the surface area available for mixing (thus sharply decreasing the timescale for homogenization). It should also be noted that the wave-breaking event shown essentially represents the time evolution at a given plane and is largely free from advection effects in the direction normal to the picture. Interfacial motions are dominated by internal gravity waves with limited mass transport capability, and hence over the 330 ms time period between the frames only an insignificant advection can take place. On the other hand, above the interface, the advective effects can be significant.

At high Ri , wave breaking is the sole entrainment mechanism, though these events are spasmodic. Figure 5 (see page 243) depicts the nature of the interface for single- and double-sided mixing at $Ri = 95$ and 90 , respectively. At such high Ri , the interface appears to be smooth and calm, except for intermittent wave breaking events. Some wave breaking was observed at Richardson numbers as high as 106. This observation is at variance with that of Hannoun & List (1988), who conjectured that at $Ri > 100$ the interface may be completely dominated by molecular-diffusive effects.

Figure 6 shows the morphology of the interface, as captured by the three-dimensional imaging system described in §2. Here, a single sweep from an experiment with $Ri = 79$ has been used to construct the spatial distribution of $\alpha = 0.5$ contours. Because of the high interfacial stability, the eddies cannot penetrate deeply into the

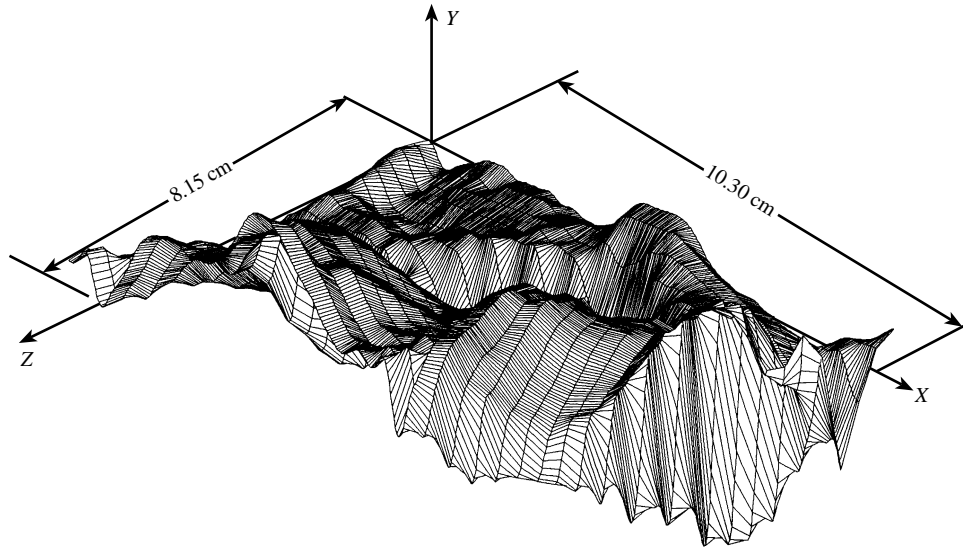


FIGURE 6. The three-dimensional structure of the interface at $Ri = 79$. X, Y is the imaging plane and Z is the sweep direction.

interface, but create undulations on the interface which propagate along it as waves. Of course, streaming motions of the eddies are possible along the valleys but, as discussed in F & H, Kelvin–Helmholtz events are expected to be rare at large Ri . As will be discussed in §4.7, plots such as figure 6 were used in examining the fractal nature of the interface.

4. Quantitative Measurements

4.1. Interfacial velocity

As outlined in §2, interfacial velocity measurements were made by tracking the vertical height $\zeta(x, t)$ of a given α -contour and by measuring its vertical position over a time $\Delta t = 334$ ms, namely $[\zeta(x, t + \Delta t) - \zeta(x, t)]/\Delta t$. Vertical velocities corresponding to different α -contours give the velocities of different isopycnals located within the interface. A plot of instantaneous vertical velocity (w) obtained for different contours within an interface, at different vertical locations, is given in figure 7. A single-sided experiment is shown, but it is typical of the behaviour of both single- and double-sided stirring cases. Figure 8 shows the variation of the r.m.s. vertical velocity $(w^2)_i^{1/2}$ for various α for the two cases in the wave breaking regime; note that the vertical r.m.s. velocity within the interface remains approximately constant in the vertical direction for both single- and double-sided stirring. This observation implies that the movement of these thin interfaces corresponds to random forcing of the first mode of internal waves, a key assumption in the model of F & H; in this (flapping) mode, all the isopycnals in the stratified layer move in phase, so that the vertical velocity within the layer remains constant. According to Carruthers & Hunt (1997), the domination of the first mode of waves in the interface occurs when $Ri_{(l)} < \pi^2$, where $Ri_{(l)} = \Delta b h / u_H^2$ is the internal Richardson number based on the interfacial-layer thickness h . Thus, thicker interfaces with large Ri_l do not display a uniform vertical velocity within the interface because of the presence of higher modes of internal waves. Experimental

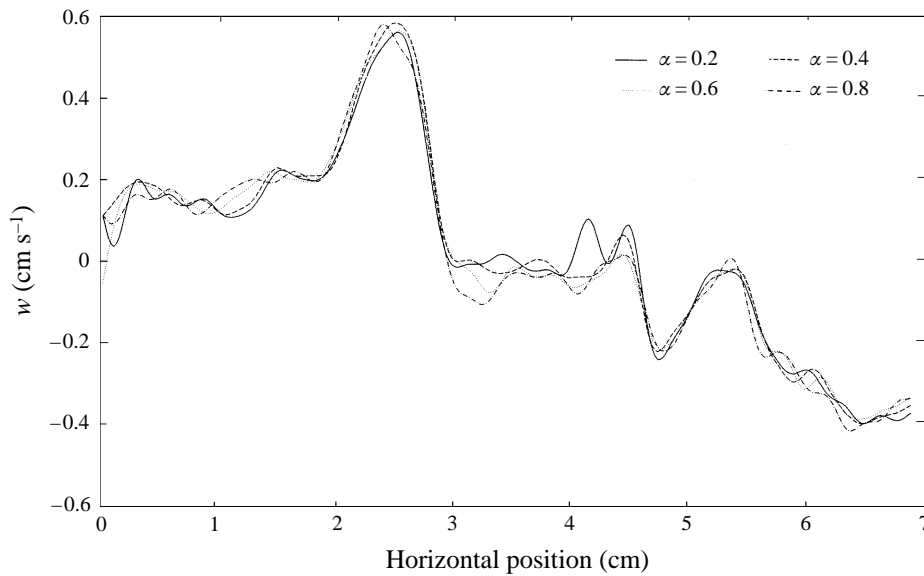


FIGURE 7. Spatial records of r.m.s. vertical velocity for various contours. The case shown is for single-sided stirring at $Ri = 51$. The measurements have been made using the LIF technique with a vertical laser sheet passing through the centre of the tank normal to the viewing direction. Here the horizontal position 3.5 cm represents the centre of the tank.

studies of Perera *et al.* (1994) showed the existence of a velocity maximum in such thick interfaces.

Figure 9 shows the variation of the normalized interfacial velocity $\overline{(w^2)_i}^{1/2}/u_H$ with Ri , based on the $\alpha = 0.5$ contour, for both cases. For the double-sided stirring, the r.m.s. velocity is about 50 % greater and has the same variation with Ri as the single-sided stirring case. The agreement between our results, based on spatial averaging, and those of Hannoun & List (1988), who used temporal velocity records at a given location, is consistent with the assumption that the interfacial turbulence field is stationary and horizontally homogeneous at least over the averaging periods. The solid and dashed lines show that $\overline{(w^2)_i}^{1/2}/u_H \propto Ri^{-1/3}$, as proposed in F & H, for single- and double-sided stirring, respectively. The proportionality constants used for these lines (1.8 and 2.6, respectively) were proposed by F & H by selecting the adjustable coefficient in their model to fit into the single-sided stirring data of Hannoun & List (1988); thence, the proportionality constant for the double sided-stirring could be predicted, without any further assumptions. The predictions of the Richardson-number power law for both cases and the proportionality constant for the double-sided stirring case are in satisfactory agreement with the experimental results.

4.2. Interfacial displacement

The displacement of isopycnals could also be computed from the digitally processed images, either by considering the deviation of the vertical interfacial position from a spatially averaged mean value or by considering the oscillations of the interface with time at a given vertical line. Both techniques were found to agree within $\pm 10\%$. The r.m.s. displacement of $\alpha = 0.5$ contours was measured for different Ri using the former technique; results are depicted in figure 10. Also shown are the single-sided stirring

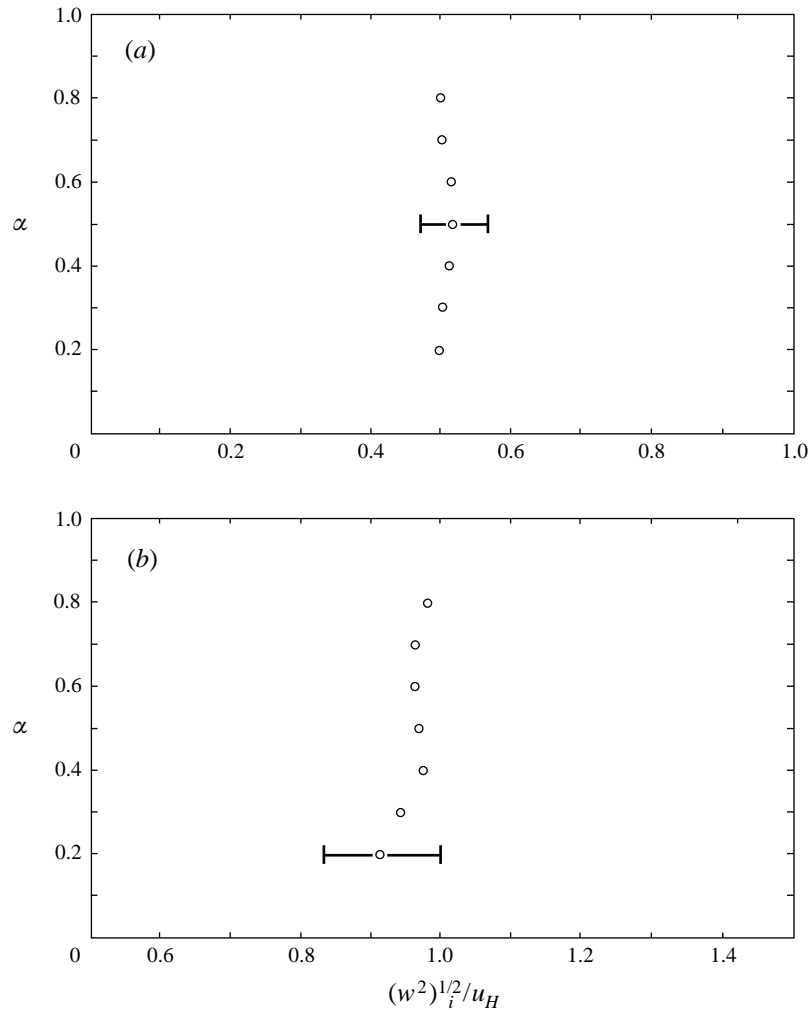


FIGURE 8. R.M.S. vertical velocity of various contours. (a) single-sided stirring at $Ri = 52$, (b) double-sided stirring at $Ri \approx 30$.

results of Hannoun & List (1988) and the predictions of the F & H model, namely $(\zeta^2)^{1/2}/L_H \sim Ri^{-5/6}$ for both single- and double-sided stirring. The coefficients 3.2 and 4.6 used in plotting these lines were also predicted by F & H. Note that a good agreement can be seen between the present measurements and those of Hannoun & List (1988) for the single-sided stirring. As with the velocity fluctuations, the r.m.s. displacements for double-sided stirring cases are greater by about 50% than for the single-sided case. In both cases these experimental results agree to within $\pm 15\%$ with the F & H model predictions.

4.3. Interfacial thickness

Careful inspection of figures 2–5 clearly reveals how the straining motions on either side of the interface and the intermittence of the mixing events cause considerable spatial variations in the interfacial layer (region with colours intermediate between red and blue). A crucial property of the interface, especially for statistical models,

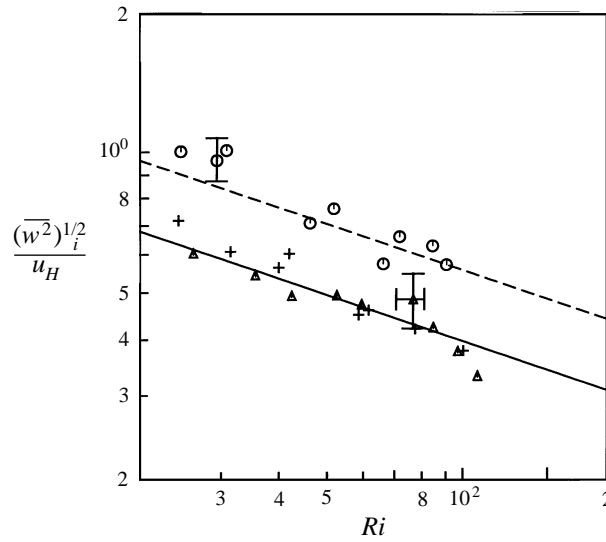


FIGURE 9. Variation of the r.m.s. interfacial velocities with Ri . The solid lines are the theoretical predictions of F & H for single-sided stirring (continuous line) and double-sided stirring (dashed line). \circ , Double-sided stirring data; \triangle , single-sided stirring data; +, single-sided stirring data of Hannoun & List (1988).

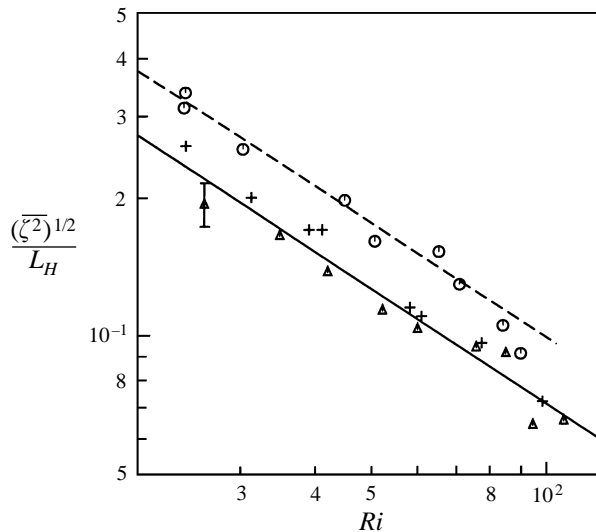


FIGURE 10. Variation of the r.m.s. interfacial displacement with Ri . The lines are the model predictions of F & H for single-sided stirring (continuous line) and double-sided stirring (dashed line). \circ , Double-sided stirring data; \triangle , single-sided stirring data; +, single-sided stirring data of Hannoun & List (1988).

is the averaged thickness as a function of Ri and other parameters. Quantitatively, the instantaneous (local) interfacial layer thickness can be defined as the vertical (Y -direction in figure 6) distance between the isopycnal contours $\alpha = 0.2$ and 0.8 ; such contours for $Ri \approx 52$ are shown in figure 11. The fact that the undulations of the two contours are approximately in phase implies that they correspond to the first mode of linear and nonlinear internal waves. Figure 11 also shows how the local

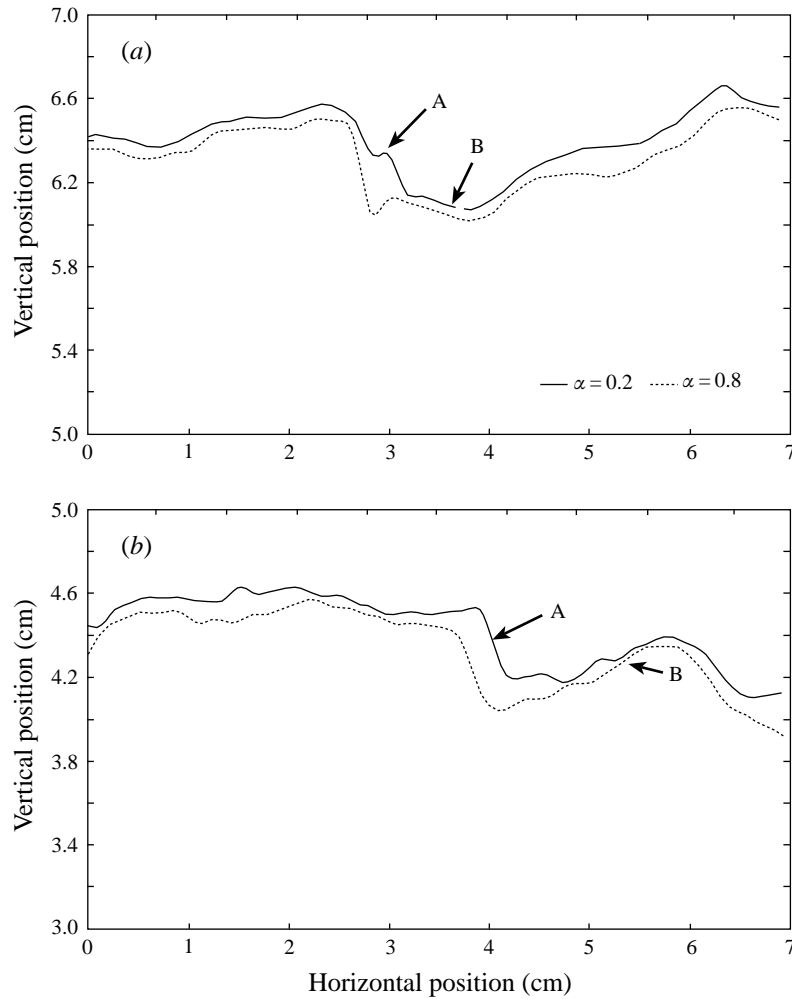


FIGURE 11. Vertical positions of several constant-density lines taken from a single video frame at $Ri \approx 52$. (a) Single-sided stirring, (b) double-sided stirring. Here the horizontal position 3.5 cm represents the centre of the tank.

interfacial-layer thickness varies by about a factor 5 between where the waves are steep and break (marked A on the figure) and where the interface is strained on the downstream slope (marked B) of a travelling wave. The variation of the average thickness (defined in §2) over a range of $Ri (> 20)$ is shown in figure 12. Note that $h/L_H = 0.27 \pm 0.04$, over the range investigated, and h/L_H does not tend to increase or decrease significantly. The ratio of h and the depth of the turbulent layer (half the distance between the grids) is an order of magnitude smaller than h/L_H . These values of h are much smaller than those obtained by concentration profile measurements using travelling conductivity probes, which show $h/L_H \sim 1$ (Crapper & Linden 1974). Hannoun & List (1988) were the first to note this disparity, which was attributed to the slow response of the measuring probes to the surrounding density variations as a result of slow replenishment of fluid at the probe tip; a fluid blob attached to the probe tip is dragged along with the moving probe, thus making the probe response sluggish. Note that the interfacial thickness, which according to the present

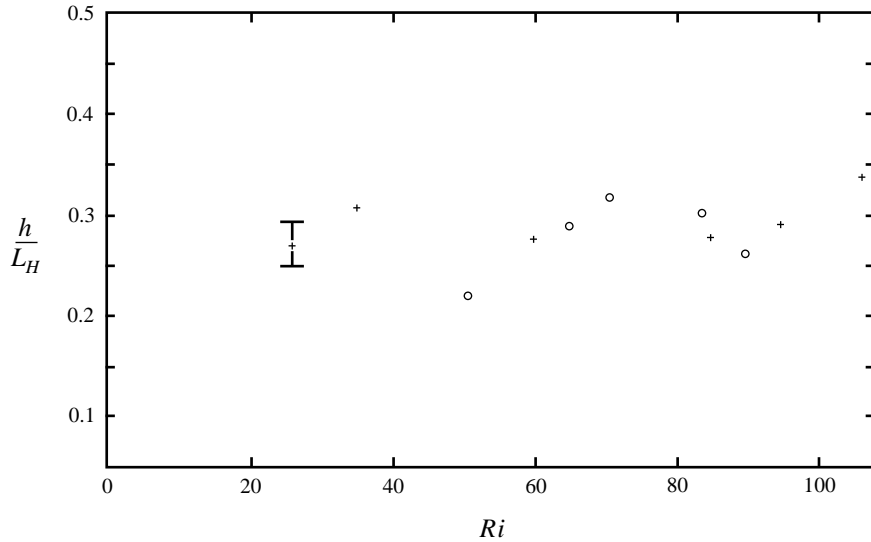


FIGURE 12. Variation of the normalized interfacial-layer thickness with Ri : +, double-sided stirring data; o, single-sided stirring data.

measurements is of the order of 0.5 cm, is much greater than the resolution of the image processing system, which for a typical field of view was 0.023 cm. The fact that the earlier interfacial thickness measurements of Hannoun & List (1988) had resolution problems for high values of Ri (> 50) explains some of the differences between theirs and the present measurements; they found a decreasing trend of h/L_H with Ri for higher Ri .

4.4. Spectra and dominant scales

Information on the discontinuities present in a function and its derivatives can be obtained from the spectra in the wavenumber (k) or frequency (ω) domain at large k or ω . If the function has discrete singularities in its n th derivative (in our case these might be inversions of isopycnals), then the spectra should take the form $f(k) \sim k^{-2(n+1)}$ or $f(\omega) \sim \omega^{-2(n+1)}$, respectively. Thus, the interfacial displacement contours $\zeta(x, t)$ for a density interface with breaking waves (i.e. with discontinuities in the zeroth derivative) can be expected to have a k^{-2} or ω^{-2} spectrum. The Fourier transforms and hence the power spectrum for $\zeta(x, t)$ were obtained using the interfacial displacement records based on $\alpha = 0.5$ contours. Typical one-dimensional wavenumber spectra $E(k_1)$ for low- and intermediate- Ri cases for both the single- and double-sided stirring cases are shown in figure 13. Note that at low Ri the exponent of spectra k_1^{-P} is not constant but its mean value over a range of intermediate scales $6 < k_1 < 60 \text{ cm}^{-1}$ is about $P = 2.0 \pm 0.4$. At small scales the exponent is somewhat less than 2. At large Ri , the wave-breaking activities are less frequent and the interface is calmer in smaller scales. This appears to be characterized by a spectral slope of -2 in a narrower k_1 range. Using the plots of $E(k_1)$, the variance-preserving spectral forms $k_1 E(k_1)$ were calculated, from which the horizontal wavenumber of the dominant disturbances of the interface was inferred (by locating the wavenumbers corresponding to the peaks). A plot of the normalized dominant wavenumber $k_d L_H$ as a function of Ri is shown in figure 14; the best fit line indicates $k_d L_H \approx 2.8$. Thus the dominant disturbance

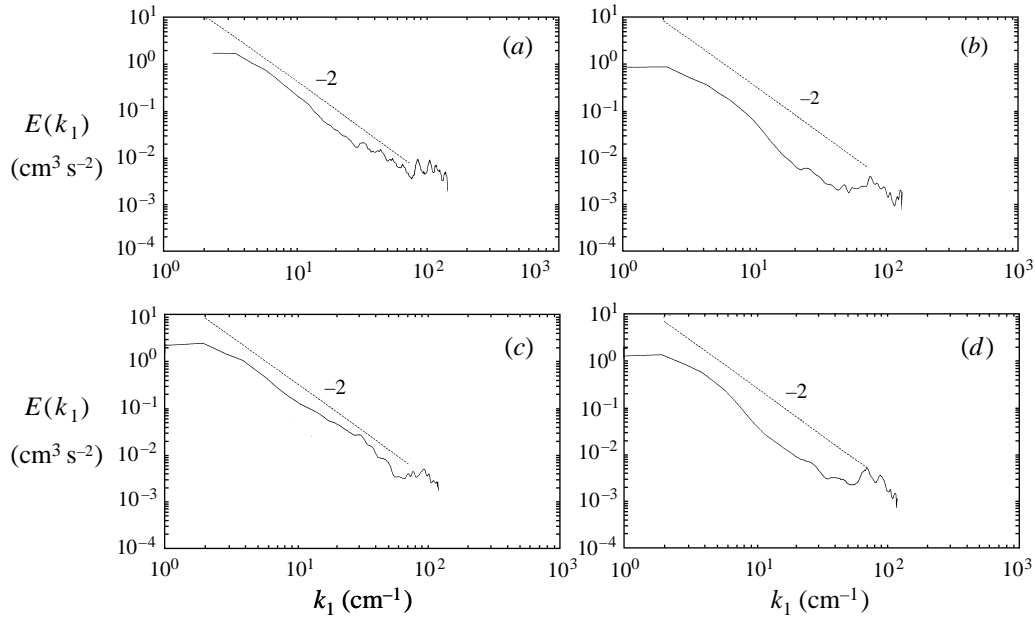


FIGURE 13. Wavenumber spectra of interfacial displacements: (a) single-sided stirring, $Ri = 26$; (b) single-sided stirring, $Ri = 52$; (c) double-sided stirring, $Ri = 30$; (d) double-sided stirring, $Ri = 65$.

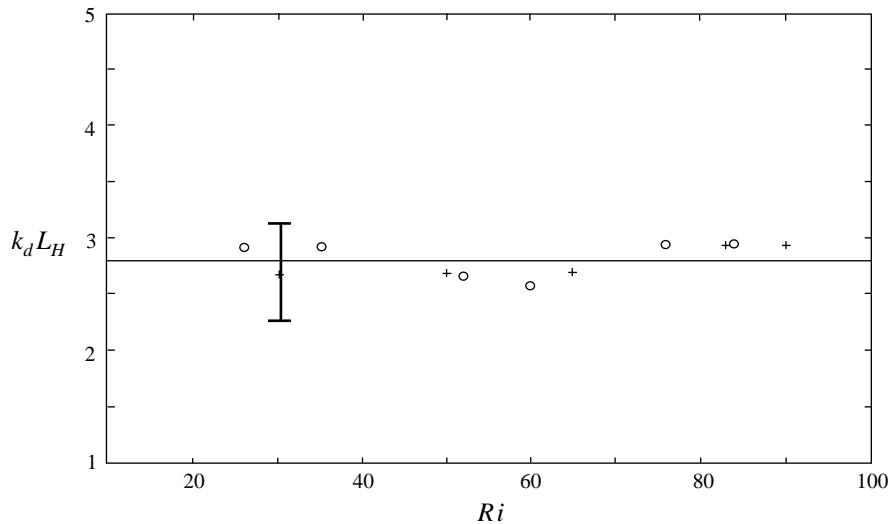


FIGURE 14. Variation of the normalized dominant wavenumber with Ri : +, double-sided stirring; \circ , single-sided stirring.

wavelength λ_d does not vary with Ri and is of the same order as the lengthscale of turbulence above the interface $\lambda_d \sim 2.2L_H$.

The above finding is consistent with the earlier observation about the lengthscale of the large eddies deflecting (and squashing) on the interface and the distance they slosh over. Observations and the above measurements indicate that at moderately high Ri , large eddies, as they impinge and flatten on the interface, may not directly

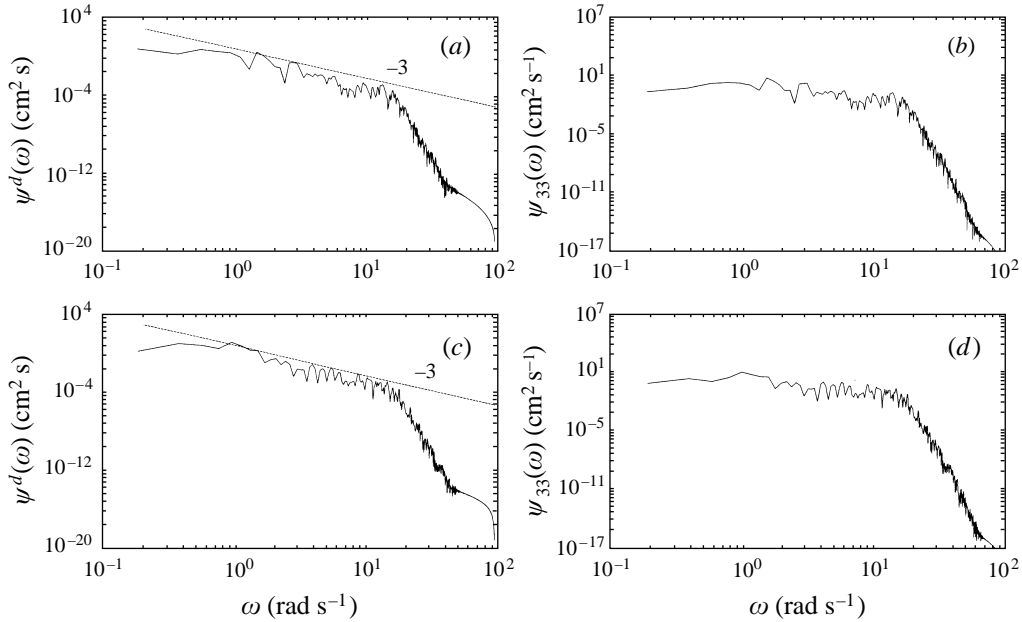


FIGURE 15. Frequency spectra for $Ri \approx 52$: (a) displacement, single-sided stirring; (b) vertical velocity, single-sided stirring; (c) displacement, double-sided stirring; (d) vertical velocity, double-sided stirring.

cause entrainment; rather they control, by their horizontal stirring motions, the extent of the spreading and the travel distance of the nonlinear waves on the interface.

Plots of frequency spectra of interfacial displacement $\zeta(t)$, $\psi^d(\omega)$, and of the vertical velocity $\psi_{33}(\omega)$ calculated using the time variation of $\zeta(t)$ at a given location are shown in figures 15(a)–(d). Also plotted on the graphs are lines with -3 slope, based on the proposal of Hannoun & List (1988) that $\psi^d(\omega)$ should have a -3 slope consistent with the degradation of the first mode of interfacial waves; this prediction is due to Phillips (1977), and does not take into account the presence of background turbulence. In the present experiments, over the range $1 < \omega < 12$ (or $4 < k_1 < 60$), it is found that the spectrum has a self-similar form, and can be represented by the equation $\psi^d \propto \omega^{-P_d}$, where $P_d \approx 2.2 \pm 0.2$. This is close to the value of 2, which is consistent with the notion that smaller waves are being advected by the longer (breaking) waves and turbulence. (Note that the spectrum with $P_d = 3$, as suggested by Hannoun & List 1988, is not kinematically congruous with steep waves having the wavenumber spectrum of figure 13.)

The vertical velocity of linear waves w is related to the displacement $\zeta(x, t)$ by $w = \partial\zeta/\partial t$; it is expected that this relation applies to the weakly nonlinear waves, and therefore, $\psi_{33}(\omega) = \omega^2\psi^d(\omega)$, or $P_3 = P_d - 2$, where the vertical velocity spectrum is assumed to have the form $\psi_{33} \propto \omega^{-P_3}$. The experimental results show that $P_3 \approx 0.2$ for $1 < \omega < 12$, which agrees with the above prediction. Note that for $P_3 \rightarrow 0$ the spectrum represents a series of delta functions in the physical space; this is approximately what is observed in figure 7. For $\omega > 20$ noise corrupts the signal, and so it is not possible to compare the high frequency range of the spectrum with the F & H model.

4.5. Interfacial gradient Richardson number

In all the experiments, quite high bulk Richardson numbers were used ($Ri > 10$), which is tantamount to using high interfacial gradient Richardson numbers, $Ri_g = (db/dz)/(du/dz)^2$. Note that if $h/L_H = 0.3$ is used and if the interfacial velocity shear exerted by eddies sloshing over the interface is parameterized as u_H/h , then $Ri_g \approx 0.3Ri$. This implies that the ‘mean’ value of Ri_g within the interface hardly falls below the critical value of, say, $1/4$ required for the production of turbulence within the interface by straining motions of eddies. As mentioned, K-H instabilities resulting from such instabilities are typically absent at the interface. Observations, nevertheless, indicate that within the interface turbulence is produced in the form of local instabilities, and hence the local Ri_g should drop below the critical value in certain regions. F & H argued that the local Ri_g can be much smaller than the mean Ri_g (calculated from db/dz , L_H and u_H), because of the large local strain rates induced by the growing amplitudes of resonant internal waves. Rapid decreases of Ri typically occur in localized patches of the stratified layer, as described by Phillips (1977, p. 219).

In a limited number of single-sided stirring experiments, the local Ri_g within the interface was measured by using the special Richardson number probe discussed in §2. Interfaces with thicknesses greater than the 2.7 mm resolution of the probes were selected for the measurements (the average interfacial-layer thickness could be changed by changing the depth of the mixed layer). Care was taken to avoid the exposure of the probe volumes to the upper turbulent layer, wherein Ri_g is very small. This was done by initially placing the probe volumes somewhat below the interface and by letting the interface deepen into the probing area; the density readings from the probes were monitored and the data segments contaminated by the exposure to the upper turbulent mixed layer were eliminated. Figure 16 shows the instantaneous Ri_g recorded for an experiment with $Ri = 70$. Note that Ri_g frequently drops below the critical value of $1/4$, which may lead to turbulence and overturning, as indicated by the negative Ri_g values. The measurements also show that the local gradient Richardson number within the interface can be much smaller than the Richardson number based on bulk parameters, conducive for overturning instabilities, and is highly variable possibly as a result of varying strain field of internal waves.

4.6. Fractal dimension

As is evident from Sreenivasan (1991), fractal geometry can be a versatile tool in obtaining information on fluid interfaces. Kolmogorov (1958) introduced the capacity dimension D_k (now known as the Kolmogorov capacity; see Vassilicos & Hunt 1991) which is defined in terms of the minimum number of elements $N(d)$ of size d required to ‘cover’ the intersection of a signal with a line or a curve on a plane or a surface in three-dimensional space. D_k is a measure of the space-filling nature of a line or a surface. For signals that demonstrate self-similarity over many lengthscales it is found that $N(d) \sim d^{-D_k^{(i)}}$ as $d \rightarrow 0$, where $D_k^{(i)}$ may be non-integer with the following limits: $0 < D_k^{(1)} < 1$, $1 < D_k^{(2)} < 2$, $2 < D_k^{(3)} < 3$ in the three cases, respectively. Different fractal dimensions D_L, D_A can also be obtained by measuring the length of the line $L(\delta)$ or the area of the surface $A(\delta)$, so that $L \sim \delta^{-D_L}$ or $A \sim \delta^{-D_A}$. The theory of Farmer, Otte & Yorke (1983) (see also Vassilicos & Hunt 1991) has shown that $D_L < D_k^{(2)}$. For smooth lines and surfaces, $D_L = 1$ and $D_A = 2$; for example, for a space-filling spiral $0 < D_k^{(1)} < 1$ but $D_L = 1$.

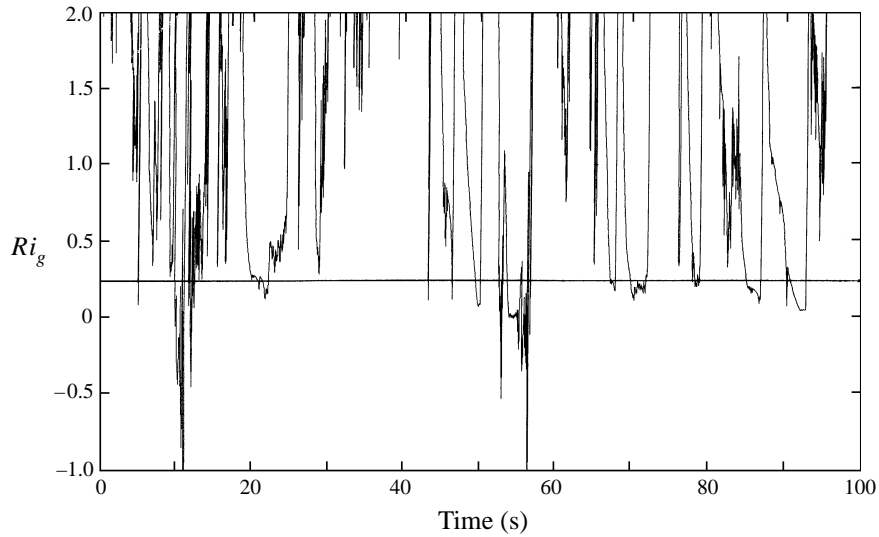


FIGURE 16. Variation of the gradient Richardson number, Ri_g , with time. The case shown is single-sided stirring, $Ri = 70$, $h \approx 0.7$ cm. The solid line is the critical value $1/4$. Negative values of Ri_g indicate overturning events.

However, for a line or surface that is everywhere fractal (in the qualitative sense of Mandelbrot 1982 or more technically has non-integer Hausdorff dimension), $D_L > 1$ and $D_A > 2$.

Note that $D_k^{(i)}$ increases as the irregularities (or ‘fragmentation’ or ‘roughness’, in the terminology of Redondo & Linden 1990) of the signal become increasingly space filling over a large range of lengthscales. Also $D_k^{(i)}$ needs to be defined for one or more ranges of lengthscales, e.g. $\delta_1 \ll \delta \ll \delta_2$ and $\delta_2 \ll \delta \ll \delta_3$, and may have different values for $\delta \ll \delta_2$ and $\delta \gg \delta_2$. For the case of a one-dimensional discontinuous signal obtained by an intersection with a multi-dimensional function, Vassilicos & Hunt (1991) proved that the connection between $D_k^{(1)}$ and the exponent of a one-dimensional power spectrum, if $E(k_1) \propto k_1^{-P}$, is such that $D_k^{(1)} = 2 - P$. They also showed why a ‘good’ measure for $D_k^{(1)}$ is more readily obtainable than a ‘good’ measure for P from a turbulent signal at moderate and low values of the Reynolds number (or high values of Ri). Note that a general relationship between P and $D_k^{(2)}$ or $D_k^{(3)}$ has not been proved nor is there any general mathematical proof that, for the same three-dimensional surface, different sections and cuts lead to any simple relationship between $D_k^{(i)}$ and $D_k^{(i-1)}$. However, Sreenivasan (1991) has found experimentally that $D_k^{(i)} \approx D_k^{(i-1)} + 1$.

Scalar interfaces in unstratified turbulent flows have been shown to have a fractal self-similar nature (Sreenivasan 1991). These studies have shown that for various classes of turbulent flows of high Reynolds number $u_H L_H / \nu > 10^2$ (jets, wakes, clouds, etc.), where ν is the kinematic viscosity, the fractal capacity dimension $D_k^{(3)}$ based on iso-scalar contours in two dimensions tends to assume a constant value of 2.33, while for intersections $D_k^{(1)} = 0.33$ for scales in the inertial range. This illustrates that self-similarity between different scales exists not only within a given type of flow, but the same measure of self-similarity occurs in various classes of turbulent flows. Simulations by Vassilicos & Hunt (1991) show that where measurements of $D_k^{(1)}$ are non-integer then the surface is either a fractal surface with discontinuities in

derivatives or a smooth surface with distinct accumulation points, which, following Moffatt (1984), may be produced by eddies with highly oscillating internal flows such as smooth spiral motions. They also noted that if the random function or disturbance consists of isolated singularities of its magnitude, then $D_k^{(i)}$ ($i = 1, 2$) and the spectral exponent P take integer values; in that case the function is not globally fractal. However, for our one-dimensional spectral results (§4.4), it was shown that $1.6 < P < 2.4$. Therefore, it is not possible to derive from these measurements any information about the space filling or fractal nature of the interface. The fact that P is close to 2 shows that the variations of density in this range of scales are those of a sharp discontinuous interface.

It remains an open question as to whether signals derived from turbulent flows are also fractal in the Hausdorff sense, so that D_L and D_A are non-integer. Measuring interfaces with density stratification requires similar techniques to those developed for passive scalar interfaces. However, the fractal dimension of the former are different because a stratified interface is governed by local dynamics that are different from scalar interfaces. As in the case of unstratified flows, it is expected that the iso-concentration lines within stratified interfaces should reveal some useful information pertinent to mixing within the interface because the geometry of such lines is akin to the turbulent mixing within the interface. To this end, the fractal dimension D_L of $\alpha = 0.5$ contours was determined by investigating the dependence of the length of such lines $L(d)$ on the measurement scale d (figure 17*a*), and testing whether the measurements are self-similar by plotting $\log L(d)$ against $\log(d)$. The smallest lengthscales considered were of the order of the estimated Kolmogorov scale of mixed-layer turbulence near the interface. Thus the range of scales covered the entire spectral range. From the linearity of the plot in figure 17*b*), it follows that the contour is approximately self-similar; its slope confirms that the contour has a low D_L fractal dimension, but this does not mean that the distortions have a trivial structure (as explained above). Also it should be noted again that, because of practical problems associated with the location of isoclines in wave breaking regions, certain amounts of filtering have been applied in obtaining these contours (§2).

The fractal-dimension D_L measurements shown in figure 18 were obtained from one-dimensional cuts of a two-dimensional surface, by taking averages of different cutting planes. If the surface of $D_k^{(2)}$ is isotropic, the fractal dimension corresponding to different vertical cutting planes of arbitrary orientations should be the same. Using plots such as those shown in figure 6, calculations of D_L were made using the iso-contours obtained in vertical planes of different orientations; the fractal dimension indeed showed only a little variation. For example, in a single-sided experiment with $Ri = 79$, the average value of $D_L = 1.02$, with a standard deviation of 3.7×10^{-3} , for six different sets of measurements obtained in mutually inclined planes. The measurements of D_L obtained for different Ri are shown in figure 18, as a plot of D_L versus Ri .

The measurements shown in figure 18 indicate an interesting trend of decreasing D_L with increasing Ri . At low Ri , the influence of inertial effects is dominant although the buoyancy effects play a role in mixing by controlling such aspects as the depth of penetration of the eddies; in this regime, D_L for both single- and double-sided stirring cases appears to be the same. As pointed out in §3, for $Ri \geq 35$ –40, the entrainment is completely taken over by the breaking internal waves at the interface, and hence the nature of the interface now depends on the dynamics of such waves. The results show that, for $Ri > 40$, the single- and double-sided interfaces show $D_L - 1 \approx Ri^{-0.05}$ and $D_L - 1 \approx Ri^{-0.04}$ behaviour, respectively. The higher value

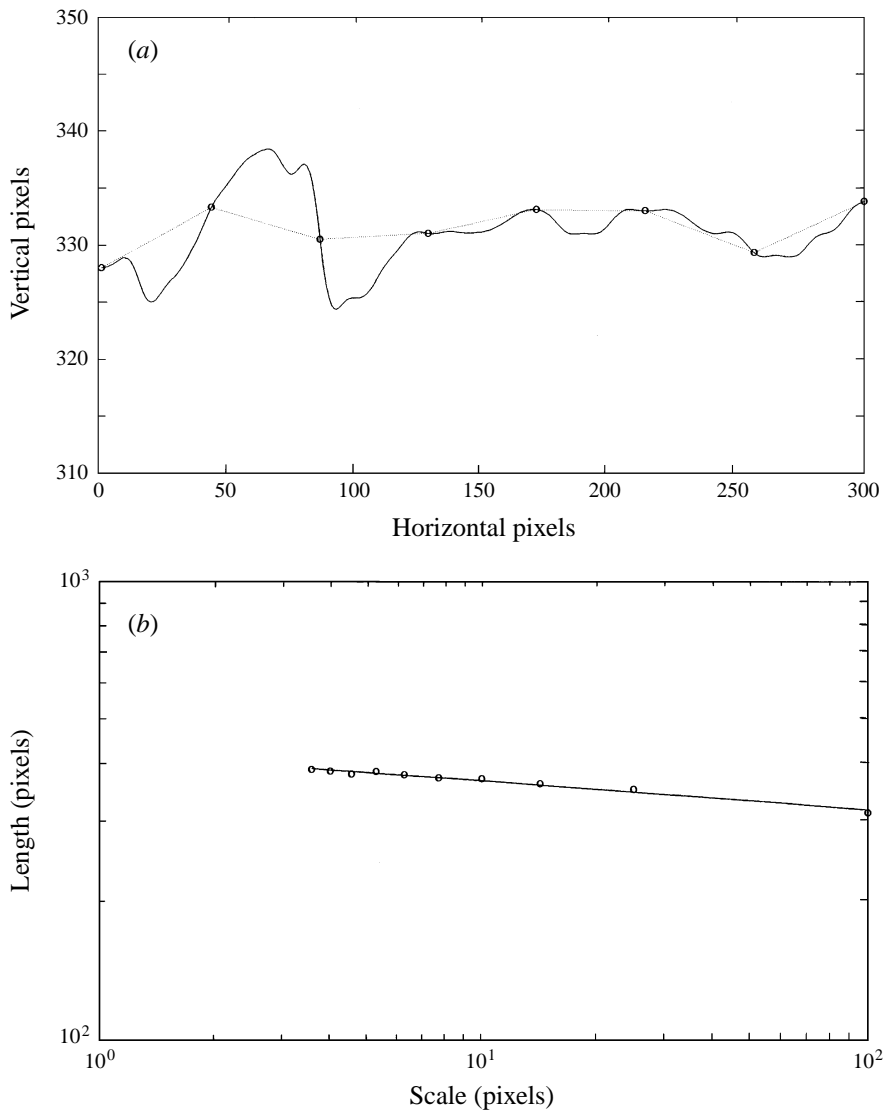


FIGURE 17. Evaluation of the fractal dimension of isopycnal contours with $\alpha \approx 0.5$. (a) Measuring the length of the contour using a 42 pixel scale. (b) The dependence of the contour length on the scale selected (each pixel resolves 0.23 mm).

of D_L for the double-sided case is consistent with the more fragmented nature of the interface, because of the associated high r.m.s. velocities and wave amplitudes. The fact that $D_L > 1$ shows that there is definitely some 'fractal-like' behaviour, but since $(D_L - 1) \ll 1$ these fractal surfaces are far from space filling. It is not surprising that the measurements show the same qualitative trend (decrease of fractal dimension with increasing Ri) as the capacity dimension measurements of Redondo & Linden (1990), but here as expected $(D_L - 1)$ is less than their corresponding value of $(D_k^{(2)} - 1)$; they found $D_k^{(2)} - 1$ approximates $Ri^{-1/2}$ behaviour over the range $10^1 < Ri < 10^3$.

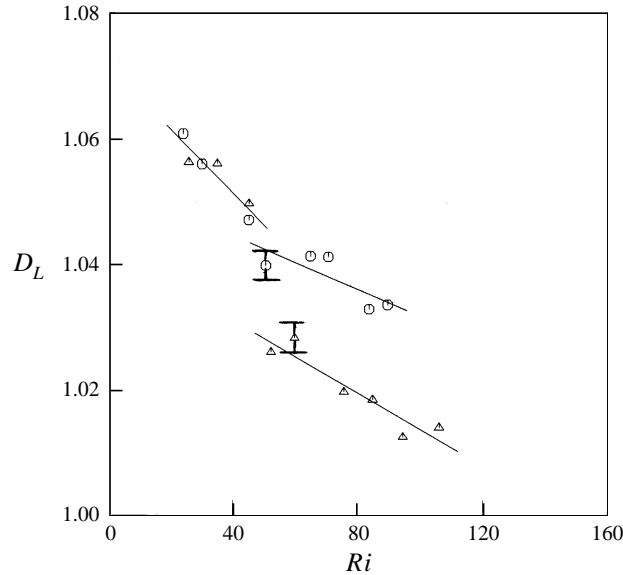


FIGURE 18. Fractal-dimension measurements D_L versus Ri : Δ , single-sided stirring; \circ , double-sided stirring.

5. Conclusions

The results of a laboratory experiment aimed toward studying the nature of turbulent mixing across shear-free thin density interfaces are described in this paper. The new features of the present work compared to the previous studies are: (i) the use of detailed laser-induced-fluorescence-based two- and three-dimensional flow visualization, thus enabling the identification of dominant mixing mechanisms at sharp density interfaces at various Richardson number Ri ranges; (ii) the measurement of the interfacial vertical velocity distribution, wave displacements and their frequency spectra for the double-sided stirring case; (iii) the measurement of the wavenumber spectra and the dominant wavenumber of the interfacial motions for both cases; (iv) the local Richardson number measurements and the demonstration of its strong time-dependent nature, including the development of instabilities; (v) interpretation of the fractal dimension measurements by considering the morphology and the displacement wavenumber spectra of the interface.

The results show that the dominant mixing mechanisms are different for different Richardson number $Ri = (\Delta b L_H / u_H^2)$ ranges, where L_H and u_H are the integral lengthscale and the r.m.s. velocity of undistorted turbulence away from the interface and Δb is the buoyancy jump across the interface. When $Ri < 15$ for single-sided stirring or $Ri < 20$ for double-sided stirring, the dominant entrainment mechanism was the impingement of eddies on the interface and splashing of heavier fluid into the mixed layer. An order of magnitude analysis shows that as Ri increases only the small-scale eddies can penetrate a distance comparable to the eddy size (the penetration distance δ of an eddy of size l in the inertial subrange with a velocity $w \sim u_H (l/L_H)^{1/3}$ can be evaluated as $w^2 \sim \Delta b \delta$, which shows that only the eddies of size $l \sim L_H Ri^{-3}$ or smaller can penetrate distances of the order of their sizes). Smaller eddies have significant horizontal velocities as they are swept by the large-scale motions near the interface. This further reduces the vertical height they can penetrate after the impingement.

At intermediate Ri the entrainment mechanism changes, and for $15 < Ri < 35$ it appears to be dominated by the shearing of interfacial-layer fluid by eddies with significant horizontal velocities that only partially penetrate the surface. Wave-like motions are present but they are continually disrupted by eddy motions. For $Ri > 35$ or so, interfacial waves and their breaking activities were prominent for both single- and double-sided cases. The speed of the waves and the distance over which they travel appeared to be determined by the large-scale motions of turbulence above the interface.

In both single- and double-sided stirring cases the interfacial layer was found to be thin, with a non-dimensional average thickness of $h/L_H \approx 0.3$, which implies the existence of a relationship between the internal Richardson number $Ri_{(I)} (= \Delta bh/u_H^2)$ and Ri as $Ri_{(I)} = 0.3Ri$. The theory of linear internal waves and estimation of the relevant scales of turbulence suggest that when $Ri_I < \pi^2$, the motion should be dominated by the first mode (Carruthers, Hunt & Turfus 1986; Carruthers & Hunt 1997). In our experiments, this inequality corresponds to the condition $Ri < 33$. The experiments reveal, however, that the interfacial displacements are approximately consistent with the first mode of internal waves at much higher values of Ri_I (of the order of 25). This discrepancy is consistent with the recent experiments carried out by Perera et al. (1994) using thick interfaces created artificially. They found that Ri_I had to be five times as large (> 50) as the theoretical value before higher modes of internal waves dominated the movement of the interface; then, as predicted by Carruthers & Hunt (1997), the vertical velocity fluctuations have a maximum value within the interface.

The normalized r.m.s. turbulent velocity and interfacial-layer isopycnal displacements showed marked variations with the bulk Richardson number which are consistent with the model predictions of F & H (1997) as $\overline{(w^2)}_i^{1/2}/u_H = 1.8Ri^{-1/3}$ and $\overline{(\zeta^2)}^{1/2}/L_H = 3.2Ri^{-5/6}$ for single-sided stirring and $\overline{(w^2)}_i^{1/2}/u_H = 2.6Ri^{-1/3}$ and $\overline{(\zeta^2)}^{1/2}/L_H = 4.6Ri^{-5/6}$, for double-sided stirring. Often, the gradient Richardson number Ri_g within the interface is much smaller than Ri , and fluctuates while frequently dropping below $1/4$ and becoming negative at times. This implies the possibility of intermittent breakdown of interfacial waves, which could be observed during the flow visualization studies. According to the analysis of Phillips (1977), the drop of Ri_g can be associated with the increase of wave amplitude during the growth of waves, which leads to local breakdown of interfacial waves.

Breaking waves produce marked discontinuities in isopycnal surfaces within the interface; hence the Fourier transformation of spatial and temporal interfacial displacement data is expected to produce k^{-2} (wavenumber) and ω^{-2} (frequency) spectra, respectively. The existence of such spectral regimes was verified experimentally. F & H (1997) have employed the above mathematical requirement for discontinuous functions in developing their entrainment model.

The fractal 'length measure' dimension D_L of selected isopycnal lines was determined as a measure of the fragmentation of the surface. Physically, highly contorted surfaces are expected to yield larger fractal dimensions and vice versa. The fact that $D_L > 1$ indicated the 'fractal-like' behaviour of the interface; the small values of the fractal dimension and the proximity of the spectral exponent close to 2, however, suggested that these fractal surfaces are far from space filling but can have complicated geometries. The fractal dimensions of single- and double-sided stirring were found to be the same for $Ri < 35$ – 40 , the parameter regime in which the interface is dominated by the inertial effects. When wave breaking takes over interfacial mixing or when

$Ri > 40$, the single- and double-sided stirring showed different fractal dimensions for the same Ri . This shows that the interfaces with single- and double-sided stirring can have morphological dissimilarities in the wave-breaking regime, possibly because of the differences in energetics.

The authors wish to thank the National Science Foundation (Fluid Dynamics and Hydraulics, International and REU programs) and the Office of Naval Research (Physical Oceanography and High Latitude Dynamics) for the financial support. Part of the work was carried out when the second author was visiting the UK Meteorological Office, the hospitality and the financial support of which are gratefully acknowledged. We greatly benefited by the stimulating discussions with Professor Daniel Jankowski, Mr Leonard Montenegro, Dr I.P. DeSilva and Dr C.Y. Ching. Three anonymous referees provided valuable comments that led to significant improvements in the manuscript.

REFERENCES

- CARRUTHERS, D. J. & HUNT, J. C. R. 1986 Velocity fluctuations near an interface between a turbulent region and a stably stratified layer. *J. Fluid Mech.* **165**, 475–501.
- CARRUTHERS, D. J. & HUNT, J. C. R. 1997 Waves, turbulence and entrainment near an inversion layer. *J. Fluid Mech.* Submitted.
- CARRUTHERS, D. J., HUNT, J. C. R. & TURFUS, C. J. 1986 Turbulent flow near density inversion layers. In *Direct and Large-Eddy Simulation of Turbulence* (ed. U. Schumann & R. Friedrich), pp. 271–290. Vieweg and Son.
- CRAPPER, P. F. & LINDEN, P. F. 1974 The structure of the turbulent density interfaces. *J. Fluid Mech.* **65**, 45–83.
- DESILVA, I. P. D. 1991 Studies of turbulent mixing in stratified turbulent patches. PhD thesis, Arizona State University.
- DESILVA, I. P. D. & FERNANDO, H. J. S. 1992 Some aspects of mixing in a stratified turbulent patch. *J. Fluid Mech.* **240**, 601–625.
- DESILVA, I. P. D., FERNANDO, H. J. S., EATON, F. & HEBERT, D. 1996 Kelvin–Helmholtz billows in nature and laboratory. *Earth Planetary Sci. Lett.* **143**, 217–231.
- DESILVA, I. P. D., MONTENEGRO, L. & FERNANDO, H. J. S. 1990 Measurement of interfacial distortions at a stratified entrainment interface. *Exps. Fluids* **9**, 174–177.
- DRAZIN, P. G. 1969 Non-linear internal waves in slightly stratified atmosphere. *J. Fluid Mech.* **36**, 433–446.
- FARMER, J. D., OTTE, E. & YORKE, J. A. 1983 The dimensions of chaotic attractors *Physica D* **7**, 153
- FERNANDO, H. J. S. 1991 Turbulent mixing in stratified flows. *Ann. Rev. Fluid Mech.* **23**, 455–493.
- FERNANDO, H. J. S. & HUNT, J. C. R. 1997 Turbulence, waves and mixing as shear free density interfaces. Part 1. Theoretical model. *J. Fluid Mech.* **347**, 197–234 (referred to herein as F & H).
- FERNANDO, H. J. S. & LONG, R. R. 1988 Experiments on steady buoyancy transfer through turbulent fluid layers separated by density interfaces. *Dyn. Atmos. Oceans* **12**, 233–257.
- HANNOUN, I. A., FERNANDO, H. J. S. & LIST, E. J. 1988 Turbulence structure near a sharp density interface. *J. Fluid Mech.* **189**, 189–209.
- HANNOUN, I. A., & LIST, E. J. 1988 Turbulent mixing at a shear-free density interface. *J. Fluid Mech.* **189**, 211–34.
- HOPFINGER, E. J. & TOLY, J. A. 1976 Spatially decaying turbulence and its relation to mixing across density interfaces. *J. Fluid Mech.* **78**, 155–175.
- HUSSAIN, A. K. M. F. & CLARK, A. R. 1981 On the coherent structures of the axi-symmetric mixing layer: a flow visualization study. *J. Fluid Mech.* **104**, 263–294.
- KIT, E., STRANG, E. J. & FERNANDO, H. J. S. 1997 Measurement of turbulence near shear-free density interfaces. *J. Fluid Mech.* **334**, 293–314.
- KOLMOGOROV, A. N. 1958 A new invariant for transitive dynamical systems. *Dokl. Akad. Nauk SSSR* **119**, 861.

- KOOCHESFAHANI, M. M. 1984 Experiments on turbulent mixing and chemical reaction in a liquid mixing layer. PhD thesis, California Institute of Technology.
- KOOCHESFAHANI, M. M. & DIMOTAKIS, P. E. 1986 Mixing and chemical reactions in a turbulent liquid mixing layer. *J. Fluid Mech.* **170**, 83–112.
- LINDEN, P. F. 1973 The interaction of vortex rings with a sharp density interface: A model for turbulent entrainment. *J. Fluid Mech.* **60**, 467–480.
- LIU, H. T., LIN, J.-T., DELISI, D. P. & ROSEN, F. A. 1977 Application of a fluorescence technique to dye-concentration measurements in a turbulent jet. NBS special publication 484. In *Proc. Symp. on Flow in Open Channels and Closed Conduits*, NBS Gaithersburg, MD, Feb. 1977.
- MCDUGALL, T. J. 1979 Measurements of turbulence in a zero-mean-shear mixed layer. *J. Fluid Mech.* **94**, 409–431.
- MCGRATH, J., FERNANDO, H. J. S. & MONTENEGRO, L. 1993 Three-dimensional spatial imaging of a density interface excited by shear-free turbulence. Rep. 93–001. Environmental Fluid Dynamics Program, Arizona State University.
- MANDELBROT, B. B. 1982 *The Fractal Geometry of Nature*. W.H. Freeman, New York.
- MOFFATT, H. K. 1984 Simple topological aspects of turbulent vorticity dynamics. *Proc. IUTAM Symposium on Turbulence and Chaotic Phenomena in Fluids* (ed. T. Tatsumi), pp. 223–230. Elsevier.
- MOFFATT, R. J. 1988 Describing the uncertainties of experimental results. *Expl Thermal Fluid Sci.* **1**, 3–17.
- MORY, M. 1991 A model of turbulent mixing across a density interface including the effect of rotation. *J. Fluid Mech.* **223**, 193–207.
- ORLANSKI, I. & BRYAN, K. 1969 Formation of the thermocline step structure by large-amplitude internal gravity waves. *J. Geophys. Res.* **74**, 6975–83.
- PAPANTONIOU, D. P. & LIST, E. J. 1989 Large scale structure in the far field of buoyant jets. *J. Fluid Mech.* **209**, 151–190.
- PERERA, M. A. J. M., FERNANDO, H. J. S. & BOYER, D. L. 1994 Turbulent mixing at an inversion layer. *J. Fluid Mech.* **267**, 275–298.
- PHILLIPS, O. M. 1955 The irrotational motion outside a free boundary layer. *Proc. Camb. Phil. Soc.* **51**, 220.
- PHILLIPS, O. M. 1959 The scattering of gravity waves by turbulence. *J. Fluid Mech.* **5**, 177–192.
- PHILLIPS, O. M. 1977 *Dynamics of the Upper Ocean*. Cambridge University Press.
- REDONDO, J. M. & LINDEN, P. F. 1990 Geometrical observations of turbulent density interfaces. *Proc. IMA Conf. on Mathematics and Computation of Deforming Surfaces*, Cambridge, Dec. 19–20, 1988 (ed. R. Perkins & R. Driehet).
- SIMPSON, J. E. & BRITTER, R. E. 1979 The dynamics of the head of a gravity current advancing over a horizontal surface. *J. Fluid Mech.* **94**, 477–95.
- SREENIVASAN, K. R. 1991 Fractals and multifractals in turbulence. *Ann. Rev. Fluid Mech.* **23**, 601–639.
- STEPHENSON, P. H. & FERNANDO, H. J. S. 1991 Turbulence and mixing in a stratified shear flow. *Geophys. Astrophys. Fluid Dyn.* **59**, 147–164.
- TOWNSEND, A. A. 1976 *The Structure of Turbulent Shear Flows*. Cambridge University Press.
- TURNER, J. S. 1968 The influence of molecular diffusivity on turbulent entrainment across a density interface. *J. Fluid Mech.* **33**, 639–656.
- VASSILICOS, J. C. & HUNT, J. C. R. 1991 Kolmogorov's contributions to the physical and geometrical understanding of small-scale turbulence and recent developments. *Proc. R. Soc. Lond. A* **434**, 183–210.